Control of qubits by shaped pulses of finite duration

Iavor I. Boradjiev and Nikolay V. Vitanov

Phys. Rev. A **88**, 013402 — Published 1 July 2013

DOI: 10.1103/PhysRevA.88.013402

Control of qubits by shaped pulses of finite duration

Iavor I. Boradjiev[1,2,*] and Nikolay V. Vitanov[1]

[1]*Department of Physics, Sofia University, James Bourchier 5 blvd, 1164 Sofia, Bulgaria*
[2]*Institute of Solid State Physics, Bulgarian Academy of Sciences, Tsarigradsko chaussée 72, 1784 Sofia, Bulgaria*

(Dated: June 13, 2013)

We consider the interaction of a two-state quantum system with a class of pulses of finite temporal duration. The pulse shape function $f(t)$ of such a pulse is necessarily a nonanalytic function of time, with discontinuous derivatives at the turn-on and turn-off times. The excitation line width — the excited-state population versus the detuning — is determined primarily by the magnitude of the jumps of the derivative $f^{(n)}(t)$ at the points of nonanalyticity, where n is the order of the first discontinuous derivative; this nonanalyticity shows up in the n-th superadiabatic basis. The excitation line width for such pulses exhibits weak power broadening — it scales up as $\Omega_0^{1/(n+1)}$, where Ω_0 is the peak Rabi frequency of the transition: $\Omega(t) = \Omega_0 f(t)$. As a specific example, we consider the power-of-sine class $f(t) = \sin^n(\pi t/T)$ $(0 \leqq t \leqq T)$ and a truncated Gaussian pulse, and we compare their excitation line widths with the well-known excitation profile of the rectangular pulse (the Rabi formula). We find that, because of the reduced power broadening, the $\sin^n$ and truncated Gaussian pulses may accelerate manipulation of qubits compared to rectangular pulses. The reason is that the lower power broadening allows one to use higher Rabi frequency, and hence shorter pulse duration, without affecting significantly other closely lying states.

PACS numbers: 32.80.Qk, 32.70.Jz, 32.80.Xx, 33.80.Be

I. INTRODUCTION

Quantum information processing with atom-like qubits (trapped atoms and ions, doped solids, quantum dots, superconducting qubits, etc.) is usually performed by driving pulses of rectangular shape, which have a well-defined duration T and on-resonance Rabi frequency

$$\Omega(t) = \Omega_0 \quad (0 \leqq t \leqq T), \tag{1}$$

and $\Omega(t) = 0$ otherwise. The transition probability between states $|0\rangle$ and $|1\rangle$ of a qubit induced by such a pulse is given by the famous Rabi formula [1–3],

$$P_{0\to1} = \frac{\Omega_0^2}{\Omega_0^2 + \Delta^2} \sin^2\left(\sqrt{\Omega_0^2 + \Delta^2}\, T/2\right), \tag{2}$$

where Δ is the qubit-field detuning. When plotted as a function of Δ the envelope of $P_{0\to1}(\Delta)$ vanishes in a Lorentzian manner, and exhibits a typical power broadening: the line width $\Delta_{\frac{1}{2}}$ (full-width-at-half-maximum) of the excitation profile $P_{0\to1}(\Delta)$ is proportional to the Rabi frequency: $\Delta_{\frac{1}{2}} = 2\Omega_0$.

The power broadening associated with the rectangular pulse shape poses a lower limit on the pulse duration, and therefore an upper limit on the speed of manipulation of the state of the qubit. For example, complete population inversion between the two qubit states is achieved by a resonant pulse of temporal area $A = \Omega_0 T = \pi$. If there are other states near one or both of the qubit states, the Rabi frequency Ω_0 of the driving pulse must be small compared to the frequency offset Δ of these states in order to avoid unwanted excitation of them. Figure 1 shows such a model case when there is a third state $|2\rangle$ near the upper state $|1\rangle$ of the two-state system of states $|0\rangle$ and $|1\rangle$. A rectangular pulse with area π will invert the transition $|0\rangle \leftrightarrow |1\rangle$ without exciting state $|2\rangle$ provided the Rabi frequency Ω_0 is far lower than the detuning Δ of state $|3\rangle$: $\Omega_0 \ll |\Delta|$. Because for a π pulse, $\Omega_0 = \pi/T$, we find from here a lower limit on the pulse duration: $T \gg \pi/|\Delta|$. The power broadening associated with the rectangular pulse shape therefore slows the quantum processors down.

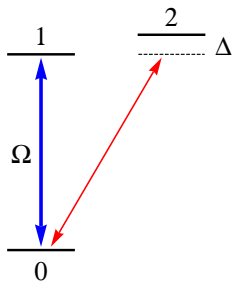

FIG. 1: (Color online) A qubit composed of states $|0\rangle$ and $|1\rangle$ driven by a resonant external field with Rabi frequency Ω_0. Unwanted excitation to state $|2\rangle$, which is coupled off-resonantly, with detuning Δ, to state $|0\rangle$ by the same driving field, is suppressed by using a sufficiently low Rabi frequency. Because a pulse with a smooth shape has lower power broadening compared to a rectangular pulse, it allows to use a larger Rabi frequency (and shorter duration) without exciting state $|2\rangle$.

The power broadening — the increase of the spectral line width of a two-level transition with the radiation intensity — is a common notion in atomic and molecular

*boradjiev@phys.uni-sofia.bg

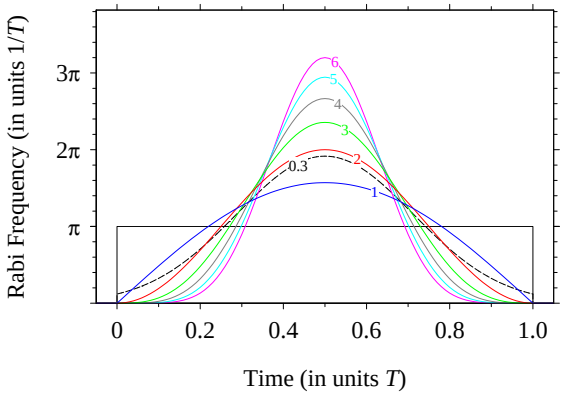

FIG. 2: (Color online) Comparison of a rectangular pulse with truncated $\sin^n(\pi t/T)$ (thick solid curves) and exponential $\exp[-(t-T/2)^2/\tau^2]$ (dashed curve, $\tau = 0.3T$) pulses. The values of n or τ/T are indicated on the respective curves. All pulses are normalized to have an area π.

spectroscopy [4, 5]. Power broadening always occurs, in particular, when a two-level atom is excited by a cw laser field. However, when the atom is exposed to a *pulsed* laser field, the extent of power broadening changes dramatically. Then it is important *how* the spectral line profile is measured [6, 7, 9, 10]. A signal collected *during* the action of the excitation pulse, e.g. by measuring the ionization produced by this pulse itself or by another ionizing laser field, still exhibits power broadening. However, in a signal measured *after* the excitation, e.g. by post-pulse fluorescence or light-induced ionization, the extent of power broadening depends very strongly on the *pulse shape* [6–9, 11]. For Gaussian pulse shapes [12, 13] there is a weak (logarithmic) power broadening, which has been demonstrated experimentally [6–8, 14]. In an even more dramatic departure from common wisdom, we have predicted recently that for smooth pulse shapes, the falling edges of which vanish as inverse powers with time (e.g., for pulse shapes that are powers of the Lorentzian function), there is *power narrowing*, i.e. the line width of the excitation profile *decreases* as the laser intensity increases [11]. The physical ground for this striking feature is the simple effect of coherent adiabatic population return [15].

These latter examples — of Gaussian and Lorentzian pulse shapes — have an infinite pulse duration. However, the circuit model of quantum computation [16] is based on circuits of one- and two-qubit gates of certain time duration, which is why rectangular pulse shapes are predominantly used.

In this paper, we use some of the ideas for reducing (with Gaussian shapes), eliminating (with hyperbolic-secant shapes) and inverting (with Lorentzian shapes) the extent of power broadening proposed and demonstrated earlier [6–9, 11], and propose to replace the rectangular pulse shape with *smoother* pulse shapes $f(t)$, still with *finite duration*, cf. Fig. 2. The main motivation for this is that smoother pulses must exhibit lower power broadening, which should allow to use higher Rabi frequency, and therefore shorter pulses, without inducing unwanted transitions to neighboring states. The pulse shape function $f(t)$ of a pulse of finite duration is necessarily a *nonanalytic* function of time, which has discontinuous derivatives at the turn-on and turn-off times, $t_\mathrm{i} = 0$ and $t_\mathrm{f} = T$. The transition probability, and hence the excitation line width, is determined mainly by the magnitude of the jumps of $f^{(n)}(t)$ at the points of nonanalyticity, where n is the order of the first discontinuous derivative. Below we shall use this feature, together with the notions of adiabatic and superadiabatic coherent population return [15], in order to estimate the transition probability induced by such partially smooth pulses of finite duration. This approach allows us to estimate the transition probability, and therefore the spectral line shape and line width, for *any* pulse of finite duration, including rectangular pulse, truncated $\sin^n$ and truncated Gaussian.

II. EXCITATION BY SMOOTH PULSES OF FINITE DURATION

A. Diabatic (bare) basis

We consider a two-state quantum system coherently excited by an external field. Its evolution is described by the time-dependent Schrödinger equation,

$$\mathrm{i}\hbar\frac{d}{dt}\mathbf{C}(t) = \mathbf{H}(t)\mathbf{C}(t), \tag{3}$$

where $\mathbf{C}(t) = [C_0(t), C_1(t)]^T$ is a column-vector with the time-dependent probability amplitudes of the unperturbed (diabatic) basis states $|0\rangle$ and $|1\rangle$. We assume that the system is initially in state $|0\rangle$: $C_0(0) = 1, C_1(0) = 0$; then the post-pulse transition probability is $P_{0\to1} = |C_1(T)|^2$.

The Hamiltonian of the two-state system in the rotating-wave approximation [2, 3] is

$$\mathbf{H}(t) = \tfrac{1}{2}\begin{bmatrix} -\Delta & \Omega(t) \\ \Omega(t) & \Delta \end{bmatrix}. \tag{4}$$

where $\Delta = \omega_0 - \omega$ is the detuning between the Bohr transition frequency ω_0 and the frequency of the driving field ω. The Rabi frequency $\Omega(t) = \Omega_0 f(t)$ parameterizes the interaction between the laser field and the atom: for an atomic electric-dipole transition $\Omega(t) = -\mathbf{d}\cdot\mathbf{E}(t)/\hbar$, where $\mathbf{d}$ is the electric dipole moment of the transition and $\mathbf{E}(t)$ is the electric field of the driving laser pulse. Here we assume that $\Omega(t)$ is real and positive because its phase is of no importance in the present context (it can be incorporated in the probability amplitudes). We further assume that $f(t)$ is a smooth function except at the turn-on time $t_\mathrm{i} = 0$ and the turn-off time $t_\mathrm{f} = T$, where $f(t)$ itself or one of its derivatives undergoes sudden jumps.

We restrict our analysis to constant detuning Δ and bell-shaped symmetric pulse shapes $f(t)$. Then the post-pulse transition probability $P_{0\to1}$ is an even function of the detuning Δ, $P_{0\to1}(-\Delta) = P_{0\to1}(\Delta)$, i.e. the excitation spectral line is symmetric [11] [22].

B. Pulse shapes

We are mainly concerned by pulse shapes that are powers of the sine function and last for half of its period, $\Omega(t) = \Omega_0 f(t)$, with

$$f(t) = \sin^n(\pi t/T) \quad (0 \leqq t \leqq T), \tag{5}$$

which are shown in Fig. 2. A pulse with a temporal area $A = \int_0^T \Omega(t)dt = \pi$ is produced for

$$\Omega_0 T = \frac{\pi\sqrt{\pi}\,\Gamma(n/2+1)}{\Gamma(n/2+1/2)}, \tag{6}$$

where $\Gamma(z)$ is the Euler's gamma function. For odd and even n we find

$$\Omega_0 T = \frac{(2k-1)!!}{2^k(k-1)!}\pi^2 \quad (n = 2k-1), \tag{7a}$$

$$\Omega_0 T = \frac{2^k k!}{(2k-1)!!}\pi \quad (n = 2k), \tag{7b}$$

with $k = 1, 2, 3, \ldots$ As the power n increases, the pulses become smoother, the nonanalyticity moves to higher derivatives. However, in order to maintain the same pulse area, the peak value of the Rabi frequency increases with n, as it follows from Eq. (6), and as it is seen in Fig. 2.

Below we use the nonanalyticities of the pulse shape function $f(t)$ at the turn-on and and turn-off times, $t_\mathrm{i} = 0$ and $t_\mathrm{f} = T$, in order to estimate the transition probability $|0\rangle \to |1\rangle$. This nonanalyticity shows up in the n-th superadiabatic basis; to this end we start by reviewing the notions of adiabatic and superadiabatic bases, and adiabatic and superadiabatic coherent population return [15].

C. Adiabatic basis, adiabatic evolution and sudden transition

1. Adiabatic basis

The adiabatic states are the (time-dependent) eigenstates of the Hamiltonian (4). The transformation matrix, which is formed by them, links the original diabatic basis to the adiabatic one: $\mathbf{C}(t) = \mathbf{R}(\vartheta_1(t))\mathbf{A}_1(t)$, where

$$\mathbf{R}(\vartheta_1) = \begin{bmatrix} \cos\vartheta_1 & \sin\vartheta_1 \\ -\sin\vartheta_1 & \cos\vartheta_1 \end{bmatrix}, \tag{8}$$

with

$$\vartheta_1(t) = \tfrac{1}{2}\arctan\frac{\Omega(t)}{\Delta} \quad (0 \leqq \vartheta_1(t) \leqq \pi/4). \tag{9}$$

The subscript 1 is introduced in anticipation of the superadiabatic bases, which will be used below; the adiabatic basis is a superadiabatic basis of order 1. Because $\Omega(t_\mathrm{i}) = \Omega(t_\mathrm{f}) = 0$ and $\Delta = \mathrm{const}$, we have $\vartheta_1(t_\mathrm{i}) = \vartheta_1(t_\mathrm{f}) = 0$, and hence

$$\mathbf{R}(t_\mathrm{i}) = \mathbf{R}(t_\mathrm{f}) = \mathbf{I}. \tag{10}$$

In other words, the diabatic and adiabatic bases coincide at t_i and t_f, and therefore, the post-pulse transition probabilities in the two bases are equal; then the choice of basis for calculation of $P_{0\to1}$ is just a matter of convenience. The Hamiltonian in the adiabatic basis reads $\mathbf{H}_1 = \mathbf{R}^\dagger\mathbf{H}\mathbf{R} - \mathrm{i}\mathbf{R}^\dagger\dot{\mathbf{R}}$, or explicitly,

$$\mathbf{H}_1(t) = \tfrac{1}{2}\begin{bmatrix} -\varepsilon_1(t) & -2i\dot\vartheta_1(t) \\ 2i\dot\vartheta_1(t) & \varepsilon_1(t) \end{bmatrix}, \tag{11}$$

where the nonadiabatic coupling $2\dot\vartheta_1(t)$ and the eigenvalues splitting $\varepsilon_1(t)$ are

$$2\dot\vartheta_1(t) = \frac{\Delta\dot\Omega(t)}{\Omega(t)^2+\Delta^2}, \tag{12a}$$

$$\varepsilon_1(t) = \sqrt{\Omega(t)^2+\Delta^2}. \tag{12b}$$

2. Adiabatic evolution

By definition, the evolution is adiabatic if there are no transitions between the adiabatic states; then the probability amplitudes can only acquire time-dependent phases in the course of the evolution. The condition for adiabatic evolution requires that

$$|\dot\vartheta_1(t)| \ll \varepsilon_1(t). \tag{13}$$

Then the terms $\dot\vartheta_1(t)$ in Eq. (11) can be neglected, the Hamiltonian (11) becomes diagonal, $\mathbf{H}_1^a(t) = -\varepsilon_1(t)\boldsymbol{\sigma}_z/2$ (with $\boldsymbol{\sigma}_z$ being the Pauli's z matrix), and the propagator contains only phase factors,

$$\mathbf{U}_1^a(t_\mathrm{f}, t_\mathrm{i}) = \begin{bmatrix} \mathrm{e}^{\mathrm{i}\eta_1} & 0 \\ 0 & \mathrm{e}^{-\mathrm{i}\eta_1} \end{bmatrix}, \tag{14}$$

with

$$\eta_1 = \tfrac{1}{2}\int_{t_\mathrm{i}}^{t_\mathrm{f}} \varepsilon_1(t)dt. \tag{15}$$

Because the adiabatic states are time-dependent superpositions of the diabatic states, the populations of the latter states *may change* during adiabatic evolution, but in the end the initial populations of the diabatic states are restored because the post-pulse transition probabilities in the two bases are equal. In the adiabatic limit, both probabilities are zero and we have coherent adiabatic population return [15].

3. Sudden transition

The condition for sudden transition is the opposite to the adiabatic condition (13),

$$|\dot{\vartheta}_1(t)| \gg \varepsilon_1(t). \tag{16}$$

Then the terms $\pm\varepsilon_1(t)$ in Eq. (11) can be neglected, the Hamiltonian (11) becomes $\mathbf{H}_1^s(t) = \dot{\vartheta}_1(t)\boldsymbol{\sigma}_y$ (with $\boldsymbol{\sigma}_y$ being the Pauli's y matrix), and the propagator reads $\mathbf{U}_1^s(t) = \exp[-\mathrm{i}\int_{t_\delta} \mathbf{H}_1^s(t)dt]$, or explicitly,

$$\mathbf{U}_1^s(t_\delta) = \begin{bmatrix} \cos\vartheta_1^s & -\sin\vartheta_1^s \\ \sin\vartheta_1^s & \cos\vartheta_1^s \end{bmatrix} = \mathbf{R}(-\vartheta_1^s), \tag{17}$$

where t_δ is the time interval of the sudden transition, and ϑ_1^s is the change of $\vartheta_1(t)$ over this interval: $\vartheta_1^s = \int_{t_\delta} \dot{\vartheta}_1(t)dt$.

4. Example: Rectangular pulse

A sudden transition is induced by a δ-function shaped coupling: $\vartheta_1(t) \propto \delta(t - t_s)$. Such a behavior of $\vartheta_1(t)$ emerges when the Rabi frequency is a discontinuous function at $t = t_s$, as in the Rabi model (1). Taking this model as an example, we find that the discontinuity of $f(t)$ at t_i and t_f leads to jumps in $\vartheta_1(t)$ of magnitude $\vartheta_1^\mathrm{i} = \vartheta_1(t_\mathrm{i}) = \frac{1}{2}\arctan(\Omega/\Delta)$ and $\vartheta_1^\mathrm{f} = \vartheta_1(t_\mathrm{f}) = -\frac{1}{2}\arctan(\Omega/\Delta)$. At any other time, the Rabi frequency is constant and therefore $\dot{\vartheta}_1(t) = 0$, i.e. the evolution is perfectly adiabatic. The propagator in the original bare basis reads $\mathbf{U}(t_\mathrm{f}, t_\mathrm{i}) = \mathbf{R}(\vartheta_1^\mathrm{f})\mathbf{U}_1^s(t_\mathrm{f})\mathbf{U}_1^a(t_\mathrm{f}, t_\mathrm{i})\mathbf{U}_1^s(t_\mathrm{i})\mathbf{R}^T(\vartheta_1^\mathrm{i})$, and by taking Eq. (10) into account we find

$$\mathbf{U}(t_\mathrm{f}, t_\mathrm{i}) = \mathbf{U}_1^s(t_\mathrm{f})\mathbf{U}_1^a(t_\mathrm{f}, t_\mathrm{i})\mathbf{U}_1^s(t_\mathrm{i}). \tag{18}$$

Next, by taking also Eqs. (14) and (17) into account, we find for the transition probability $P_{0\to1} = |U_{10}(t_\mathrm{f}, t_\mathrm{i})|^2$ the expression

$$P_{0\to1} = \sin^2 2\vartheta_1^\mathrm{i} \, \sin^2\eta_1. \tag{19}$$

After replacing ϑ_1^i and η_1, and using the relation $\sin^2(\arctan x) = x^2/(x^2+1)$, we find exactly the Rabi formula (2). This is not surprising because for the Rabi model the assumptions for sudden evolution at t_i and t_f and adiabatic evolution in between are satisfied exactly.

5. Example: Truncated Gaussian pulse

The next example is a Gaussian pulse centered at $T/2$ with its wings truncated symmetrically at the turn-on and turn-off times $t_\mathrm{i} = 0$ and $t_\mathrm{f} = T$ (see Fig. 2),

$$\Omega(t) = \Omega_0 \exp\left[-(t - T/2)^2/\tau^2\right] \quad (0 \leqq t \leqq T), \tag{20}$$

The discontinuity of $f(t)$ at t_i and t_f causes jumps in $\vartheta_1(t)$ of magnitude $\vartheta_1^\mathrm{i} = -\vartheta_1^\mathrm{f} = \frac{1}{2}\arctan[\Omega_0 \mathrm{e}^{-T^2/(4\tau^2)}/\Delta]$. Then the transition probability is given by Eq. (19); explicitly,

$$P_{0\to1} = \frac{\Omega_0^2 \mathrm{e}^{-T^2/(2\tau^2)}}{\Omega_0^2 \mathrm{e}^{-T^2/(2\tau^2)} + \Delta^2} \, \sin^2\eta_1. \tag{21}$$

Unlike the Rabi model, this formula is only approximate because the assumption of adiabatic evolution in the time interval $[0, T]$ is only an approximation. Baring the oscillatory part, the excitation line width scales as

$$\Delta_{\frac{1}{2}} \approx \Omega_0 \mathrm{e}^{-T^2/(4\tau^2)}. \tag{22}$$

In the limit $\tau \to \infty$ the Gaussian becomes infinitely broad and the time interval $[0, T]$ cuts off only its flat top. Hence the truncated Gaussian reduces to the rectangular pulse and the transition probability (19) reduces to the Rabi formula (2); the cut-off dominates the probability completely.

For small τ ($\tau \ll T$), the discontinuity caused by the truncation has a negligible effect on the transition probability because $\mathrm{e}^{-T^2/(2\tau^2)} \ll 1$. Then the truncated pulse differs very little from a Gaussian pulse of infinite duration, which has been studied in detail elsewhere [12, 13]. Then the transition probability is determined primarily by the condition for nonadiabatic evolution, which reads [13]

$$\Omega_0 \gtrsim \frac{\Delta}{2} \, \mathrm{e}^{\frac{27}{4}\Delta^2\tau^2\epsilon^2}, \tag{23}$$

where ϵ is a small number measuring the deviation from perfect adiabaticity [13]. This condition shows a logarithmic power broadening of the excitation line width.

We conclude that for large τ, the line width suffers from power broadening nearly as much as the rectangular pulse. For small τ, the line width increases due to deteriorating adiabaticity, cf. Eq. (23). This suggests the existence of some optimal value τ_opt, for which the excitation line width is minimal; we have estimated this value to be $\tau_\mathrm{opt} \approx 0.3T$.

D. Superadiabatic bases

The treatment for the smooth pulses of finite duration of Eq. (5) follows the same template, with two important differences. First, the sudden transitions are calculated in the appropriate superadiabatic basis, of order $n+1$, in which the respective coupling has a δ-function behavior at the turn-on and turn-off times t_i and t_f, as a result of the nonanalyticity of the pulse shape $f(t)$. Second, we assume that between t_i and t_f there are no transitions in the $(n+1)$-st superadiabatic basis, which amounts to superadiabatic evolution; therefore, unlike the Rabi model, the solutions are only *approximate* because the evolution away from the singularities is not perfectly superadiabatic.

1. Lowest superadiabatic basis

The superadiabatic bases of different order n are generated by diagonalization of the Hamiltonian in the respective preceding superadiabatic basis of order $n-1$, starting from the adiabatic basis, for which we take $n=1$. Thus the superadiabatic basis of order 2 is formed of the eigenstates of the adiabatic Hamiltonian (11). Before proceeding we make the phase transformation

$$\mathbf{F} = \begin{bmatrix} \mathrm{e}^{-\mathrm{i}\pi/4} & 0 \\ 0 & \mathrm{e}^{\mathrm{i}\pi/4} \end{bmatrix}, \tag{24}$$

which does not change the probabilities. It casts the adiabatic Hamiltonian (11) in the form of the original bare-basis Hamiltonian (4), $\mathbf{H}_1(t) \to \mathbf{H}_2(t) = \mathbf{F}^\dagger \mathbf{H}_1(t)\mathbf{F}$, with the correspondences $\Delta \to \varepsilon_1(t)$, $\Omega(t) \to 2\dot{\vartheta}_1(t)$ and $\mathbf{C}(t) \to \mathbf{A}_1(t)$. Now we can repeat all the calculations of Sec. II C, with the replacements

$$\vartheta_1(t) \to \vartheta_2(t), \tag{25a}$$
$$\varepsilon_1(t) \to \varepsilon_2(t), \tag{25b}$$
$$\mathbf{A}_1(t) \to \mathbf{A}_2(t), \tag{25c}$$
$$\mathbf{H}_1(t) \to \mathbf{H}_2(t), \tag{25d}$$
$$\eta_1 \to \eta_2. \tag{25e}$$

Of particular significance are the superadiabatic coupling $\dot{\vartheta}_2(t)$ and splitting $\varepsilon_2(t)$,

$$\dot{\vartheta}_2(t) = \frac{\varepsilon_1(t)\ddot{\vartheta}_1(t) - \dot{\varepsilon}_1(t)\dot{\vartheta}_1(t)}{\varepsilon_1(t)^2 + 4\dot{\vartheta}_1(t)^2}, \tag{26a}$$

$$\varepsilon_2(t) = \sqrt{\varepsilon_1(t)^2 + 4\dot{\vartheta}_1(t)^2}. \tag{26b}$$

The conditions for superadiabatic and supersudden evolution read

$$|\dot{\vartheta}_2(t)| \ll \varepsilon_2(t) \quad \text{(superadiabatic)}, \tag{27a}$$
$$|\dot{\vartheta}_2(t)| \gg \varepsilon_2(t) \quad \text{(supersudden)}. \tag{27b}$$

If the superadiabatic coupling $\dot{\vartheta}_2(t)$ has a δ-function behavior at the turn-on and turn-off times, while it is negligibly small compared to the superadiabatic splitting $\varepsilon_2(t)$ at any time in between, the solution in the original bare basis will be similar to the Rabi model, Eq. (18),

$$\mathbf{U}(t_\mathrm{f}, t_\mathrm{i}) = \mathbf{U}_2^s(t_\mathrm{f})\mathbf{U}_2^a(t_\mathrm{f}, t_\mathrm{i})\mathbf{U}_2^s(t_\mathrm{i}), \tag{28}$$

with $\mathbf{U}_2^a(t_\mathrm{f}, t_\mathrm{i})$ and $\mathbf{U}_2^s(t_\delta)$ defined as Eqs. (14) and (17), with the subscript 1 replaced by 2.

We note that this definition of superadiabatic bases, obtained by repeated diagonalization of the Hamiltonian in the preceding superadiabatic basis, differs from earlier definitions [17], but is in accord with others [18, 19].

2. Sine pulse: approximate solution

The solution (28) is particularly suitable for the sine pulse,

$$\Omega(t) = \Omega_0 \sin(\pi t/T) \quad (0 \leqq t \leqq T), \tag{29}$$

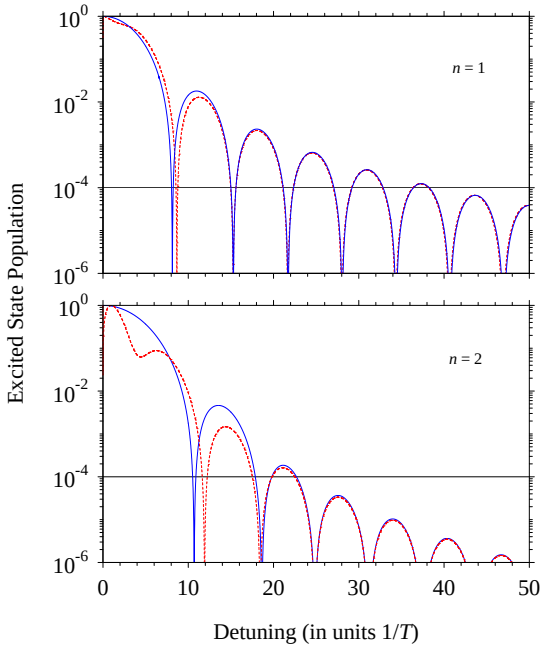

FIG. 3: (Color online) Post-pulse transition probability $P_{0\to1}$ vs the detuning Δ for the sine pulse shape of Eq. (29) (top) and the $\sin^2$ shape of Eq. (32) (bottom). The pulse area is $A = \pi$ in both cases, which according to Eq. (6) means that $\Omega_0 = \pi^2/2$ for $n = 1$ and $\Omega_0 = 2\pi$ for $n = 2$. The solid lines are obtained by numerical integration of the Schrödinger equation and the dashed lines are the analytic approximations (31) (top) and (34) (bottom).

because it has a discontinuous first derivative, and therefore, δ-function singularities in the superadiabatic coupling at the turn-on and turn-off times $t_\mathrm{i} = 0$ and $t_\mathrm{f} = T$. The magnitudes of the jumps of $\vartheta_2(t)$ at t_i and t_f are

$$\vartheta_2(t_\mathrm{i}) = -\vartheta_2(t_\mathrm{f}) = \frac{1}{2}\arctan\frac{\pi\Omega_0}{\Delta^2 T}. \tag{30}$$

The approximate transition probability for the sine pulse (29) reads

$$P_{0\to1} = \frac{\pi^2\Omega_0^2}{\pi^2\Omega_0^2 + \Delta^4 T^2}\cos^2\eta_2, \tag{31}$$

with $\eta_2 = \frac{1}{2}\int_{t_\mathrm{i}}^{t_\mathrm{f}} \varepsilon_2(t)dt$. Although this approximate formula bears many similarities to the Rabi formula (2), there is one essential difference: this is the term with Δ^4 in the pre-factor, which signals reduced power broadening, to which we shall return in the next section.

Figure 3 (top frame) compares the analytic approximation (31) for the transition probability $P_{0\to1}$ to the exact numerical values for a sine pulse with an area π. The analytic formula (31) describes remarkably accurately both the amplitude and the phase of the oscillations in $P_{0\to1}$, except for small detuning where the assumption for superadiabatic evolution between the singularities is not fulfilled well.

3. Sin^2 pulse: approximate solution

The same approach allows us to obtain the naked singularities for any other $\sin^n$ pulse shape of Eq. (5) by going, iteratively, to the $n+1$-st superadiabatic basis. For the $\sin^2$ pulse shape,

$$\Omega(t) = \Omega_0 \sin^2(\pi t/T) \quad (0 \leqq t \leqq T), \tag{32}$$

we repeat the procedure described above but for the $n = 3$ superadiabatic basis by replacing all subscripts "1" by "2" and all subscripts "2" by "3". The magnitude of the jumps of $\vartheta_3(t)$ at t_i and t_f are

$$\vartheta_3(t_\mathrm{i}) = \vartheta_3(t_\mathrm{f}) = \frac{1}{2}\arctan\frac{2\pi^2\Omega_0}{\Delta^3 T^2}. \tag{33}$$

Thereby we find the following approximate expression for the transition probability:

$$P_{0\to1} = \frac{4\pi^4\Omega_0^2}{4\pi^4\Omega_0^2 + \Delta^6 T^4}\sin^2\eta_3, \tag{34}$$

with $\varepsilon_3(t) = \sqrt{\varepsilon_2(t)^2 + 4\dot{\vartheta}_2(t)^2}$ and $\eta_3 = \frac{1}{2}\int_{t_\mathrm{i}}^{t_\mathrm{f}}\varepsilon_3(t)dt$. We note the power Δ^6 in the pre-factor of Eq. (34), which signals a further reduction of the power broadening.

Figure 3 (bottom frame) compares the analytic formula (34) for the transition probability $P_{0\to1}$ to the exact numerical values for a $\sin^2$ pulse with an area π. Formula (34) describes very well the amplitude and the phase of the oscillations in $P_{0\to1}$ for fairly large detunings, while it is not as good for small detuning where the assumption for superadiabatic evolution is not fulfilled very well. In particular, formula (34) is very accurate around the quantum computation benchmark value 10^{-4}.

4. Higher superadiabatic bases

In the general case of $\sin^n$ pulse shape, Eq. (5) with arbitrary n, the transition probability is given by a similar formula as for the sin and $\sin^2$ pulses above; it is calculated in the superadiabatic basis of order $n+1$, wherein the singularity in the $\sin^n$ pulse shape emerges: the superadiabatic coupling $\dot{\vartheta}_{n+1}(t)$ has a δ-function behavior at the turn-on and turn-off times t_i and t_f. If it is negligibly small compared to the superadiabatic splitting $\varepsilon_{n+1}(t)$ at any other time in between, the solution in the original bare basis will be similar to Eq. (28),

$$\mathbf{U}(t_\mathrm{f}, t_\mathrm{i}) = \mathbf{U}^s_{n+1}(t_\mathrm{f})\mathbf{U}^a_{n+1}(t_\mathrm{f}, t_\mathrm{i})\mathbf{U}^s_{n+1}(t_\mathrm{i}), \tag{35}$$

with $\mathbf{U}^a_{n+1}(t_\mathrm{f}, t_\mathrm{i})$ and $\mathbf{U}^s_{n+1}(t_\delta)$ defined as Eqs. (14) and (17), with the subscript 1 replaced by $n+1$.

If $\vartheta_{n+1}(t_\mathrm{f}) = -\vartheta_{n+1}(t_\mathrm{i})$, as for the power-of-sine pulse shapes (5) with odd n, we find from here for the transition probability the expression

$$P_{0\to1} = \sin^2 2\vartheta^\mathrm{i}_{n+1}\cos^2\eta_{n+1} \quad (\text{odd } n). \tag{36}$$

If $\vartheta^\mathrm{f}_{n+1} = \vartheta^\mathrm{i}_{n+1}$, as for the shapes (5) with even n, we find

$$P_{0\to1} = \sin^2 2\vartheta^\mathrm{f}_{n+1}\sin^2\eta_{n+1} \quad (\text{even } n). \tag{37}$$

It is therefore important to calculate the magnitude of the jumps of $\vartheta_{n+1}(t)$ at t_i in the $(n+1)$-st superadiabatic basis; the value is readily found,

$$\vartheta^\mathrm{i}_{n+1} = \tfrac{1}{2}\arctan\frac{n!\pi^n\Omega_0}{\Delta^{n+1}T^n}. \tag{38}$$

By using the relation $\sin^2(\arctan x) = x^2/(x^2+1)$, we find

$$\langle P_{0\to1}\rangle = \frac{(n!\pi^n\Omega_0)^2}{(n!\pi^n\Omega_0)^2 + (\Delta^{n+1}T^n)^2}, \tag{39}$$

where we have dropped the oscillatory factors $\cos^2\eta_{n+1}$ and $\sin^2\eta_{n+1}$ with the dynamical phase η_{n+1} in Eqs. (36) and (37), and $\langle P_{0\to1}\rangle$ denotes the amplitude of these Rabi-like oscillations. Obviously, Eq. (39) reduces to the Rabi formula (2) for $n = 0$, as it should be the case because the rectangular shape is the $n = 0$ case of the $\sin^n$ shapes (5). We note that $\sin^n$ pulses have been discussed, in a different context, by Yatsenko *et al.* [20].

5. Condition for superadiabatic evolution

It is important to estimate the condition for superadiabatic evolution during the excitation in order to have a criterion for validity of our results. For the $\sin^n$ pulse shapes (5) a simple calculation gives

$$|\Delta| \gtrsim \left(\frac{n!n\pi^{n+1}\Omega_0}{2T^{n+1}}\right)^{\frac{1}{n+2}} \propto \Omega_0^{\frac{1}{n+2}}. \tag{40}$$

E. Excitation line width

Equation (39), which is one of the central results in this paper, allows us to find immediately the excitation line width, which we define as the detuning range $(-\Delta_{\frac{1}{2}}, \Delta_{\frac{1}{2}})$ wherein $\langle P_{0\to1}\rangle > \frac{1}{2}$. Obviously,

$$\Delta_{\frac{1}{2}} = \left(\frac{n!\pi^n\Omega_0}{T^n}\right)^{\frac{1}{n+1}} \propto \Omega_0^{\frac{1}{n+1}}. \tag{41}$$

It is important that this value, as can easily be verified, is larger than the boundary value in Eq. (40) for the superadiabatic approximation. This implies that our approach provides the correct value for the excitation line width.

The positive power of the peak Rabi frequency Ω_0 in Eq. (41) indicates power broadening; however, it is much reduced compared to the Rabi model. For sin, $\sin^2$ and

$\sin^3$ pulses we have, respectively,

$$\Delta_{\frac{1}{2}} = \left(\frac{\pi\Omega_0}{T}\right)^{\frac{1}{2}} \propto \Omega_0^{\frac{1}{2}} \quad (n=1), \tag{42a}$$

$$\Delta_{\frac{1}{2}} = \left(\frac{2\pi^2\Omega_0}{T^2}\right)^{\frac{1}{3}} \propto \Omega_0^{\frac{1}{3}} \quad (n=2), \tag{42b}$$

$$\Delta_{\frac{1}{2}} = \left(\frac{6\pi^3\Omega_0}{T^3}\right)^{\frac{1}{4}} \propto \Omega_0^{\frac{1}{4}} \quad (n=3). \tag{42c}$$

As the smoothness parameter n increases, the power broadening rapidly diminishes. We also note that, for fixed time duration T, the peak Rabi frequency Ω_0 required to produce a certain pulse area A increases with n, as seen in Eq. (6) and Fig. 2. These two opposite tendencies imply that for a fixed value of the pulse area A, the right-hand-side of Eq. (41) possesses a minimum at a certain value of n [note that for a fixed A, Ω_0 depends on n, as in Eq. (6) for $A=\pi$]. As A increases this optimum n slowly increases, from $n=1$ for $A \lesssim 3\pi$, to $n=2$ for $A \sim 5\pi$, to $n=3$ for $A \sim 15\pi$, etc.

F. Quantum computation benchmark

Besides the line width at half-maximum, formula (39) allows us to estimate the detuning Δ_{qc} beyond which the transition probability falls below the value 10^{-4}, which is the usual quantum computing benchmark error. By requiring that $\langle P_{0\to1}\rangle = \epsilon$, with $\epsilon = 10^{-4}$, we find for a π pulse, for which the peak Rabi frequency is given by Eq. (6), that

$$\Delta_{qc} = \frac{\pi}{T}\left(\frac{n!\,\Gamma(n/2+1)}{\Gamma(n/2+1/2)}\sqrt{\pi(1/\epsilon-1)}\right)^{\frac{1}{n+1}}. \tag{43}$$

Δ_{qc} has a shallow minimum in the range $n = 4, 5, 6$. We have already seen in Fig. 3 that the analytic formula (39) describes very accurately the transition probability $P_{0\to1}$ around the quantum computation benchmark error value 10^{-4} for $n = 1$ and 2. We have found that this conclusion remains valid also for larger n, i.e. Eq. (43) can be considered as a very accurate estimate.

III. EXAMPLES

A. Two-state system

In order to verify the scaling law (41) for the $\sin^n$ pulse shapes of Eq. (5), we have plotted in Fig. 4 the post-pulse transition probability $P_{0\to1}$ versus the detuning, and the scaling, linear with respect to $(\Omega_0 T)^{1/(n+1)}$, of the vertical axis allows us to view the dependence of Eq. (41) as linear. Baring the Rabi oscillations around resonance, a linear behavior is established in each frame, which confirms the universal scaling law (41). Note the difference

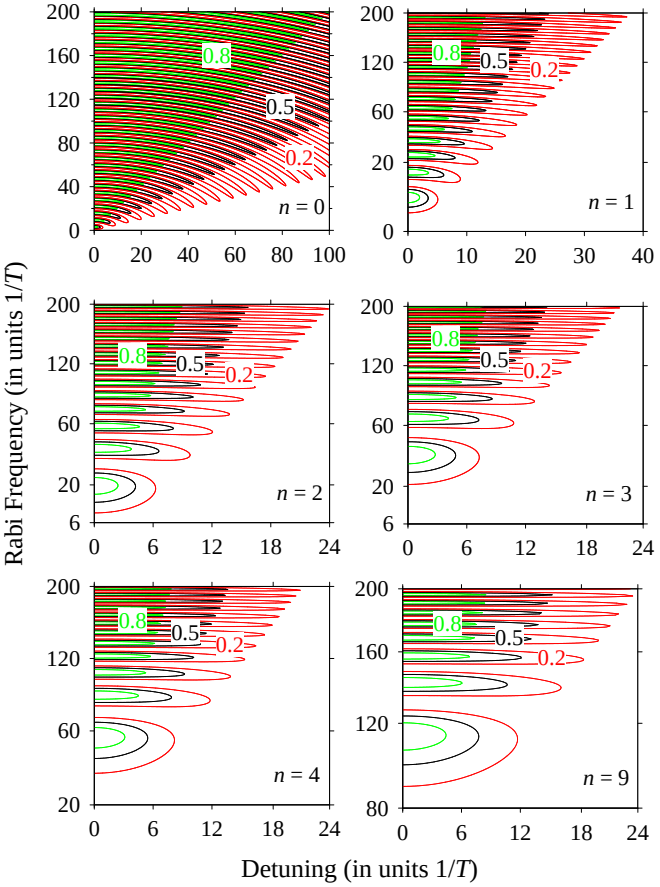

FIG. 4: (Color online) Numerically calculated post-pulse transition probability $P_{0\to1}$ vs the detuning Δ and the peak Rabi frequency Ω_0 for $\sin^n$ pulse shapes of Eq. (5), with n indicated in each frame. The vertical axes are scaled linearly with respect to the corresponding quantities $(\Omega_0 T)^{1/(n+1)}$, which allows us to verify the dependence $\Delta_{\frac{1}{2}} \propto \Omega_0^{1/(n+1)}$ stemming from Eq. (41), which should appear linear in each corresponding frame.

in the detuning range for the different shapes. All $\sin^n$ pulses produce much narrower excitation profiles than the rectangular pulse ($n=0$). The narrowest profiles are obtained for $n=3$ and 4, in line with our analytic results above.

Figure 5 shows the post-pulse transition probability $P_{0\to1}$ versus the detuning for several $\sin^n$ pulse shapes of Eq. (5) with pulse area π. The transition probability for the rectangular pulse ($n=0$) does not fall below the mark 10^{-4} (even not below 10^{-3}) in the displayed detuning range (it does so for $\Delta \gtrsim 300/T$), while the $\sin^n$ pulse shapes of Eq. (5) achieve this even for moderately large detunings, e.g. for $\Delta \lesssim 22/T$ for the $\sin^4$ pulse. As discussed above, the increase of this detuning range for larger n ($n=9$) is due to the larger peak Rabi frequency Ω_0 needed to produce an area π.

Figure 6 shows the post-pulse transition probability $P_{0\to1}$ versus the detuning for several truncated Gaussians (each with an area of π) with different values of τ. The

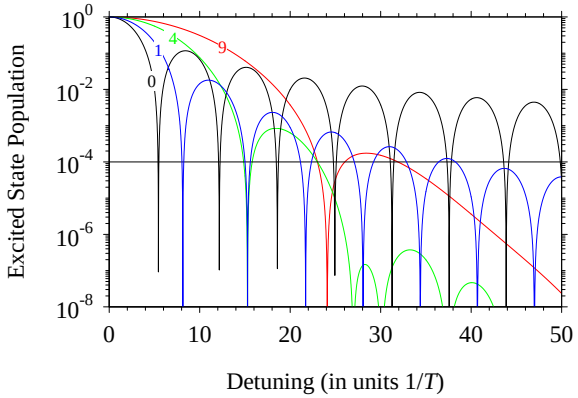

FIG. 5: (Color online) Numerically calculated post-pulse transition probability $P_{0\to1}$ (in logarithmic scale) vs the detuning Δ for the $\sin^n$ pulse shapes of Eq. (5). The respective value of n for each curve is indicated in the figure. The pulse area of each pulse is π.

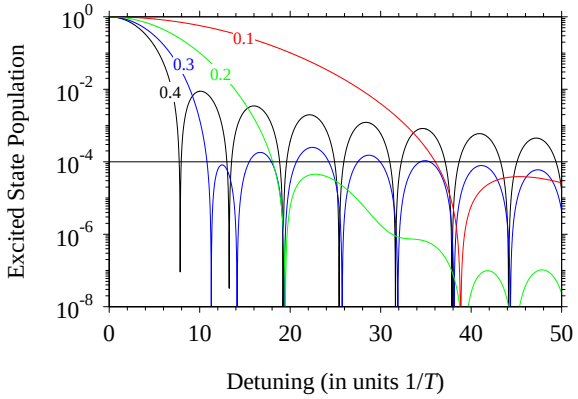

FIG. 6: (Color online) The same as Fig. 5 but for truncated Gaussians (20) with pulse area π. Here the labels denote the value of τ for each curve.

figure demonstrates the existence of an optimal value of τ at around $0.3T$, in good agreement with the analysis in Sec. II C 5. Above it the excitation profile broadens due to the jumps of the coupling at the turn-on and turn-off times. Below it the excitation profile broadens due to the increased peak Rabi frequency needed to keep the pulse area equal to π for a squeezed pulse.

B. Three-state system

The main difference of the partly smooth $\sin^n$ pulse shapes and the truncated Gaussians compared to the rectangular pulse — the narrower excitation profile $P_{0\to1}(\Delta)$ — is most advantageous in the presence of other states close to one of the qubit states, the excitation of which must be avoided. The V-system of Fig. 1 is the simplest model system, which allows us to examine the selectivity of excitation $|0\rangle \to |1\rangle$. State $|2\rangle$ is situated near state $|1\rangle$, and the pulse driving the transition

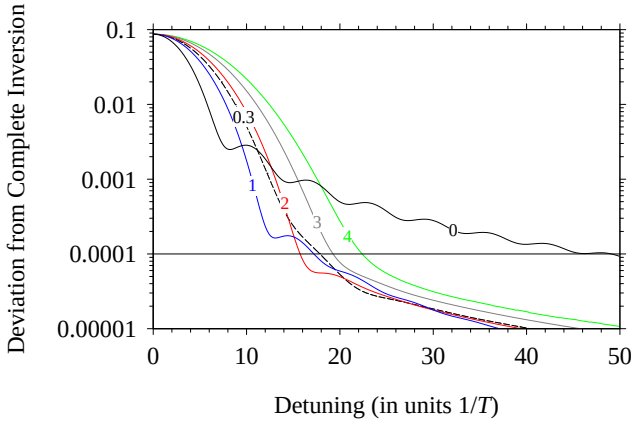

FIG. 7: (Color online) Numerically calculated deviation of the post-pulse transition probability $P_{0\to1}$ from 1 (in logarithmic scale) vs the detuning Δ in the three-state V-system shown in Fig. 1 for the $\sin^n$ pulses of Eq. (5) (thick solid curves), and for the truncated Gaussian pulse of Eq. (20) (dashed curve). The respective values of n for the $\sin^n$ pulses and $\tau = 0.3T$ for the truncated Gaussian are indicated on each curve. The peak Rabi frequency for the transition $|0\rangle \leftrightarrow |1\rangle$ is such that the pulse area of each pulse is π. The pulse area for the transition $|0\rangle \leftrightarrow |2\rangle$ is 0.3π for each pulse.

$|0\rangle \leftrightarrow |1\rangle$ can excite also the transition $|0\rangle \leftrightarrow |2\rangle$ (generally with a different Rabi frequency). If the driving field is resonant with the transition $|0\rangle \leftrightarrow |1\rangle$ and detuned from the transition $|0\rangle \leftrightarrow |2\rangle$ by a detuning Δ, the Hamiltonian of this V system reads

$$\mathbf{H} = \frac{1}{2}\begin{bmatrix} 0 & \Omega(t) & \beta\Omega(t) \\ \Omega(t) & 0 & 0 \\ \beta\Omega(t) & 0 & 2\Delta \end{bmatrix}, \qquad (44)$$

where the number β is the ratio of the coupling strength of the transition $|0\rangle \leftrightarrow |2\rangle$ relative to the one for the transition $|0\rangle \leftrightarrow |1\rangle$; in the simulations we take $\beta = 0.3$. Such a situation arises in the excitation of many atoms and ions with hyperfine structure (with energy splittings in the GHz range) by nanosecond pulses. In order to avoid the unwanted excitation of state $|2\rangle$ one has to use a sufficiently small peak Rabi frequency Ω_0 compared to the detuning Δ. If we want to invert the transition $|0\rangle \leftrightarrow |1\rangle$ by a π pulse, then the objective to suppress unwanted excitation of state $|2\rangle$ imposes an upper limit on Ω_0, and hence a lower limit on the time duration T. Figure 7 shows numerical simulations, which demonstrate the performance of different pulse shapes for this purpose. A sufficiently large detuning Δ eventually decouples the unwanted state $|2\rangle$ from the dynamics and leaves the π pulse acting upon, and inverting the desired transition $|0\rangle \leftrightarrow |1\rangle$. The figure shows, for different pulse shapes, how large the detuning Δ must be so that the transition $|0\rangle \leftrightarrow |1\rangle$ does not "feel" the presence of state $|2\rangle$. The best performance is achieved with a truncated Gaussian with $\tau = \tau_{\rm opt} \approx 0.3T$, and sin and $\sin^2$ pulses; for these the decoupling of state $|2\rangle$ (i.e., when its population drops

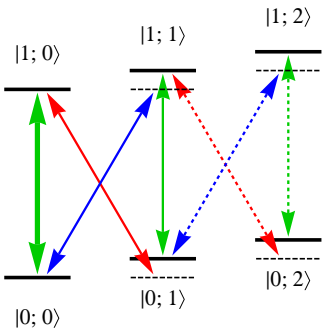

FIG. 8: (Color online) Linkage patterns for qubit transitions in a trapped ion. Each qubit state $|0\rangle$ and $|1\rangle$ is split into a ladder of infinitely many harmonic sublevels, with a splitting equal to the trap frequency ν. The notation $|q; v\rangle$ stands for the qubit state $|q\rangle$ dressed with v phonons. Qubit driving at the carrier frequency (thick arrow) may induce unwanted transitions to other (off-resonant) vibrational states (thin arrows). The solid arrows indicate the transitions that are taken into account in the numerical simulations.

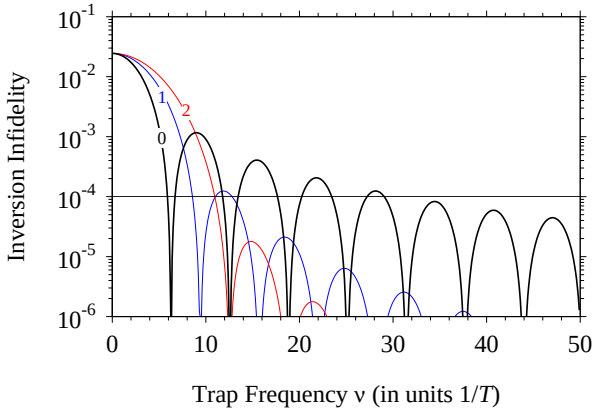

FIG. 9: (Color online) Numerically calculated error in the population inversion $|0; 0\rangle \to |1; 0\rangle$, resulting from the action of a rectangular pulse (thick curve), sine and $\sin^2$ (thin curves) pulses in the four-state system of Fig. 8. The area of each pulse is equal to π.

below the 10^{-4} benchmark) occurs for detunings that are by a factor of over 3 lower compared to the one for the rectangular pulse. For a fixed detuning Δ, this implies that sin and $\sin^2$ pulses and a truncated Gaussian with $\tau_{\rm opt}$ can invert the qubit, with an error less than 10^{-4}, over three times faster than a rectangular pulse.

C. Multistate system

The partly smooth pulses discussed above have similar advantages over the rectangular pulse in more complex multistate systems. As an example, we consider the states of an ion qubit in a linear Paul trap, which are dressed by a certain number of quantized motional quanta (phonons) [21], as shown in Fig. 8. Each qubit state is split into an infinite ladder of vibrational states, with the splitting equal to the trap frequency ν. Qubit driving at the carrier frequency (thick arrow) may induce also unwanted transitions to other (off-resonant) vibrational states (thin arrows), which must be suppressed. Again, this puts a lower limit on the pulse duration T because the Rabi frequency Ω_0 should be kept sufficiently small compared to the trap frequency ν.

The Hamiltonian of the system composed of the first four vibrational states linked with the solid arrows in Fig. 8 reads

$$\mathbf{H} = \frac{1}{2}\begin{bmatrix} 0 & \Omega_g & 0 & \Omega_b \\ \Omega_g & 0 & \Omega_r & 0 \\ 0 & \Omega_r & 2\nu & \Omega_g \\ \Omega_b & 0 & \Omega_g & 2\nu \end{bmatrix}, \qquad (45)$$

where the states are ordered as follows: $|0; 0\rangle$, $|1; 0\rangle$, $|0; 1\rangle$, $|1; 1\rangle$. Here $\Omega_g(t) = \Omega(t)$ is the Rabi frequency of the carrier transitions (associated with no change in the phonon number), $\Omega_r(t) = \eta\Omega(t)$ is the Rabi frequency of the red-sideband transition $|0; v\rangle \to |1; v-1\rangle$, and $\Omega_b(t) = \eta\Omega(t)$ is the Rabi frequency of the blue-sideband transition $|0; v\rangle \to |1; v+1\rangle$. Here η is the Lamb-Dicke parameter, which is the ratio between the sizes of the ionic wavefunction and the light field [21]. In the Lamb-Dicke limit, we have $\eta \ll 1$; we take $\eta = 0.1$.

The objective here is to drive the carrier transition $|0; v\rangle \to |1; v\rangle$ without exciting the other transitions. The problem is that the driving pulse couples all other transitions, blue- and red-sideband, albeit off-resonantly. The unwanted transitions $|0; 0\rangle \to |1; 1\rangle$ and $|1; 0\rangle \to |0; 1\rangle$ have lower Rabi frequency $\eta\Omega(t)$, which are attenuated by the Lamb-Dicke parameter η. These unwanted transitions can be eliminated by ensuring that their Rabi frequency $\eta\Omega(t)$ is far less than the trap frequency ν. This upper limit upon $\Omega(t)$ sets a lower limit on the pulse duration T, which ultimately slows the gate operation.

Figure 9 shows the error in the population inversion of the transition $|0; 0\rangle \to |1, 0\rangle$ for different pulse shapes in the presence of the other, unwanted states $|0; 1\rangle$ and $|1; 1\rangle$. The sin and $\sin^2$ pulses demand, for fixed Rabi frequency Ω_0, a factor of 3 lower trap frequency ν than a rectangular pulse; conversely, for a fixed trap frequency ν, the sin and $\sin^2$ pulses allow to use a factor of 3 higher Rabi frequency, and hence one can speed up the qubit manipulation by the same factor. Similar conclusions apply for a truncated Gaussian pulse with optimal τ.

IV. CONCLUSIONS

We have demonstrated, by using the concepts of adiabatic and superadiabatic bases, adiabatic evolution, sudden transitions and coherent population return, that the use of partly smooth pulse shapes of finite duration (powers of sine and truncated Gaussian) can speed up the manipulation of qubits for quantum information process-

ing as compared to rectangular pulses. To this end, we have derived an approximate expression for the transition probability induced by such pulses, Eq. (39), which shows that these pulses have much lower power broadening compared to rectangular pulses, Eqs. (41) and (43). In the derivation we have used the fact that the nonanalyticity of such pulses of finite duration shows up in the $(n+1)$-st superadiabatic basis, where the corresponding superadiabatic coupling has a δ-function behavior at the turn-on and turn-off times; this allowed us to readily estimate the transition probability. The much reduced power broadening of these $\sin^n$ pulses makes them superior to the rectangular pulse when there are unwanted states nearby the two qubit states: the $\sin^n$ pulses and the truncated Gaussian have much higher selectivity of excitation, which allows to use much higher values of the Rabi frequency, and hence much shorter pulse durations. We have demonstrated this speed-up in three- and four-state systems.

Acknowledgments

This work is supported by the Bulgarian NSF grant D002-90/08 and the Alexander von Humboldt Foundation.

[1] I. I. Rabi, Phys. Rev. **51**, 652 (1937).
[2] L. Allen and J. H. Eberly, *Optical Resonance and Two Level Atoms* (Dover, N.Y., 1975).
[3] B. W. Shore, *The Theory of Coherent Atomic Excitation* (Wiley, New York, 1990).
[4] R. G. Breene, *Theories of Spectral Line Shapes* (Wiley, N.Y., 1981).
[5] I. I. Sobel'man, L. A. Vainshtein and E. A. Yukov, *Excitation of Atoms and Broadening of Spectral Lines*, (Springer, N.Y., 1981)
[6] N. V. Vitanov, B. W. Shore, L. P. Yatsenko, K. Böhmer, T. Halfmann, T. Rickes, K. Bergmann, Opt. Commun. **199** 117 (2001).
[7] T. Halfmann, T. Rickes, N. V. Vitanov, K. Bergmann, Opt. Commun. **220** 353 (2003).
[8] A. P. Conde, L. Brandt, and T. Halfmann, Phys. Rev. Lett. **97**, 243004 (2006).
[9] N. V. Vitanov, B. W. Shore, L. P. Yatsenko, Ukr. J. Phys. V **54** 53 (2009).
[10] B. T. Torosov, G. S. Vasilev, and N. V. Vitanov, Opt. Commun. **283**, 1338 (2010).
[11] I. I. Boradjiev and N. V. Vitanov, Opt. Commun. **288**, 91 (2013).
[12] P. R. Berman, L. Yan, K.-Hwee Chiam, and R. Sung Phys. Rev. A **57**, 79 (1998).
[13] G. S. Vasilev and N. V. Vitanov Phys. Rev. A **70**, 053407 (2004).
[14] C. W. S. Conover, Phys. Rev. A **84**, 063416 (2011).
[15] M. Born and V. A. Fock, Zeitschrift fr Physik A **51**, 165 (1928); N. V. Vitanov and P. L. Knight, J. Phys. B **28**, 1905 (1995); N. V. Vitanov, J. Phys. B **28**, L19 (1995); A. Kuhn, S. Steuerwald, K. Bergmann, Eur. Phys. J D **1**, 57 (1998); B. W. Shore, Acta Physica Slovaca **58**, 243 (2008).
[16] M. A. Nielsen and I. L. Chuang, *Quantum Computation and Quantum Information* (Cambridge University Press, Cambridge, 2000).
[17] R. Lim and M. V. Berry, J. Phys. A **24**, 3255 (1991); M. V. Berry and R. Lim, ibid. **26**, 4737 (1993).
[18] N. V. Vitanov and K.-A. Suominen, Phys. Rev. A **59**, 4580 (1999).
[19] N. V. Vitanov, L. P. Yatsenko and K. Bergmann, Phys. Rev. A **68**, 043401 (2003).
[20] L. P. Yatsenko, S. Guérin, and H. R. Jauslin, Phys. Rev. A **70**, 043402 (2004).
[21] D. J. Wineland, C. Monroe, W. M. Itano, D. Leibfried, B. E. King, and D. M. Meekhof, J. Res. Natl. Inst. Stand. Technol. **103**, 259 (1998).
[22] For asymmetric pulse shapes, the excitation line profile is asymmetric too, but the basic results remain intact.